Frequency stability in AFM

THESIS

submitted in partial fulfillment of the
requirements for the degree of

MASTER OF SCIENCE
in
PHYSICS

Author :	Ruben Guis
Student ID :	S1684078
Supervisor :	G. J. Verbiest
	Prof.dr. P. G. Steeneken
2^{nd} corrector :	Dr. M.J.A. de Dood

Leiden, The Netherlands, September 21, 2020

Frequency stability in AFM

Ruben Guis

Huygens-Kamerlingh Onnes Laboratory, Leiden University
P.O. Box 9500, 2300 RA Leiden, The Netherlands

September 21, 2020

Abstract

Atomic force microscopy (AFM) is a versatile surface-sensitive technique. One of the main challenges is to expand these capabilities to also image the subsurface structure of the sample, for example by using ultrasound. Existing ultrasound methodologies often indicate the phase of the cantilever vibration as the most sensitive subsurface channel. Even if such techniques can be developed to their full potential, it remains a question how accurate and fast these methods can become. To get an idea on the possibilities, we measured the frequency stability, which is similar to the phase stability, of a cantilever in a home-built AFM. We started by making the optical detection system and tested it by measuring the thermomechanical peak of the cantilever. Then the piezo inside the cantilever holder was fixed to drive the cantilever. In AFM the resonance frequency changes due to the tip-sample interaction. However no resonator is perfect, and the resonance frequency will vary even when there is no sample at all. To characterize the smallest tip-sample interactions that can be measured, one needs to characterize the frequency stability of the cantilever without a sample. To do this we have tracked the resonance frequency using a phase-locked loop. The cantilever was driven at its resonance frequency for 2 hours. The stability of its resonance frequency was analysed using the Allan deviation. We saw that for time intervals up to 30 seconds the Allan deviation had a downwards slope of $-\frac{1}{2}$ which corresponds to white frequency modulation. The short time interval Allan deviation was lower in measurements using a PLL bandwidth of 1000Hz. From the data became clear that using a PLL bandwidth of 1000Hz instead of 100Hz, the resonance frequency was flatter in time but had spikes. The lower PLL bandwidths we used were not able to resolve these spikes, that are probably caused by the unshielded cables used in the setup. Earlier we already saw spikes in the individual photodiode signals caused by these unshielded cables. For intervals longer than 30 seconds this slope for the Allan deviation was +1 (corresponds to drift in resonance frequency). This can be attributed to environmental changes, for instance temperature fluctuations, that change the resonance frequency of the cantilever. The minimum Allan deviation was around 10^{-6}. This is 11mHz RMS deviation for the 11kHz cantilever. This is equivalent to a 0.18mdeg phase noise, which is already less than the phase-contrast caused by a 50nm gold particle buried 200nm in a soft polymer at 1MHz. The minimum Allan deviation we measured is still 3 orders of magnitude above values found in the literature for resonators with a comparable mass. Shielding cables might improve this.

Contents

CHAPTER 1
Introduction

1.1 Project Motivation

Like you can find your way in the dark by touching the walls using your hands, an Atomic Force Microscope (AFM) uses a small needle to touch a sample and feel where atoms are located.

This and similar techniques like STM and electron microscopes are used for example in lithography to verify if the surface of a chip is clean. However, the possible defect structure below the surface remains unnoticed. These impurities below the surface can change the behaviour and performance of that chip.

By knocking on the wall, you can use the resulting sound to determine whether there is a hollow space behind. We want to use the same principle at the nanoscale. By knocking on the sample with the AFM tip, we will listen to the response to gather information about what is below the surface.

If these defects in chips can be found using this knocking technique, production methods can be improved to increase chip performance.

Another interesting application would be biological imaging. It would be revolutionary to make a 3D image of the inside structure of a virus or bacterium with atomic resolution.

In this project, we will take the first steps towards this goal by building a regular AFM and measuring the frequency stability of a cantilever. After this project is finished we will expand on this and add the subsurface possibilities.

1.2 Atomic Force Microscopy

1.2.1 History and Working Principle

The invention of the scanning tunneling microscope (STM) in 1981 by Gerd Binnig and Heinrich Rohrer was a huge breakthrough in nanoscience, that even earned them the 1986 Nobel prize in physics.

STM utilises the quantum tunneling effect. When the sharp STM needle is brought close to the conducting surface and a bias voltage is applied, it becomes possible for electrons to tunnel through the barrier between the sample

and the tip. The amplitude of this tunneling current greatly depends on the distance between the tip and the sample. This means that when we use feedback on a piezo that controls the vertical separation between the sample and the tip to keep the tunneling current constant, the vertical separation is kept constant as well. Recording this feedback voltage makes it possible to determine the height. When the needle is now scanned over the surface it becomes possible to measure a height map of the sample with a precision of up to 0.001 nm in height, which is about 100 times smaller than the diameter of an atom.

Although 2D images with height information and electronic properties can be measured with sub-atomic precision using STM, the samples used have to be conducting. Therefore people kept looking for a way to be able to do this kind of measurements for non conducting surfaces.

In 1985 Binning, Quate and Gerber invented and realised the first AFM [4]. It was based on the STM, but now a conducting cantilever with a sharp tip was inserted between the sample and the STM tip. Using the standard STM measurement procedure the distance between the cantilever and the tip was determined. The distance between the cantilever tip and the sample determines the interaction strength and therefore the deflection of the cantilever. By using feedback on the sample height the deflection is kept constant. Measuring this sample feedback now also gives the height profile of the sample, but now also non conducting surfaces could be measured.

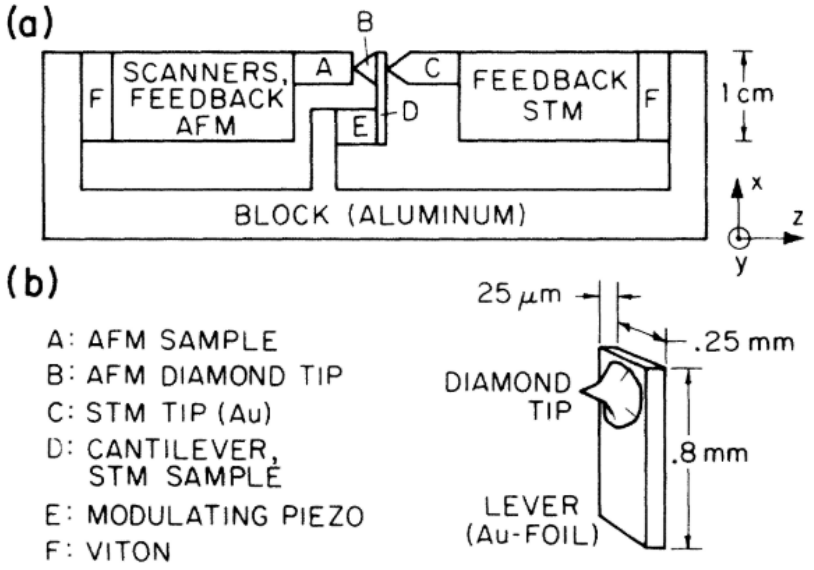

Figure 1.1: *(a) Schematic of the first working AFM [4]. A typical STM setup is used to determine the distance to a conducting cantilever beam (D). This cantilever, together with a new scanning and feedback system this system can be used to do scanning probe measurements on both conducting and non-conducting samples. (b) Legend and AFM cantilever dimensions.*

Since both STM and AFM deduce the shape of the surface by feeling the interactions with a small probe that scans over the surface, these techniques belong to the family of scanning probe microscopes (SPM).

In modern AFM setups, the STM part to read out the cantilever deflection is commonly replaced by an optical readout system. A laser beam is aimed at the cantilever. The bending of the cantilever will change the direction of reflection, which will be measured using a photodiode array. Another possibility for detection of the deflection of the cantilever is for instance interferometry. Cantilevers with a reflective coating are used for better performance.

1.2.2 Subsurface Microscopy

Currently, there are several approaches to enhance the technique even further and also gather information on atoms below the surface.

A few examples of methods to get sub-surface information with AFM are:

Magnetic Resonance Force Microscopy
The sharp tip is replaced by a small magnetic sphere (B_0 in MRI), which has a high field gradient. By resonantly flipping the spins in the sample with an RF current (B_1), due to interactions between the spins and the magnetic particle attached to the cantilever the resonance frequency and Q-factor change. Analysing this already makes it possible to measure individual electron spins [9]. Because of the magnetic interactions the tip never has to touch the surface. The high magnetic field gradient of the small magnetic particle attached to the cantilever makes sure the resonance frequency to flip the spins changes rapidly with distance from the magnet. By sending the right pulses it is possible to image spins below the surface.

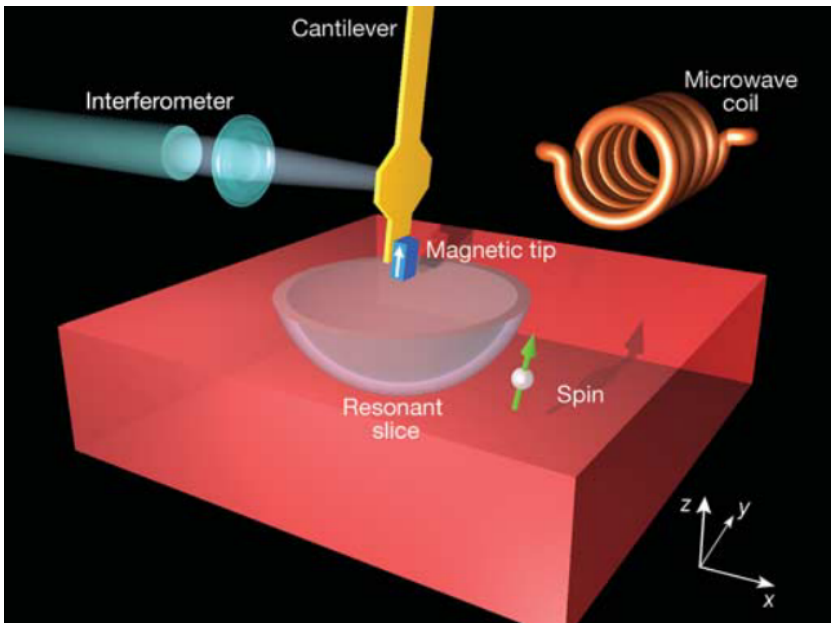

Figure 1.2: *A soft cantilever with a magnetic tip applies a magnetic field to the spins in the sample. This field makes the spins precess with the Larmor frequency, which depends on the distance from the magnetic tip via the magnetic field strength. By applying a pulse at this Larmor frequency, only spins in the resonance slice flip and change their interaction with the cantilever. By measuring this interaction, for instance with the resonance frequency of the cantilever, the location of the spins in the sample can be determined. Picture is taken from [9]*

A disadvantage to this technique is that only particles with a nonzero magnetic moment interact with the pulses and can be measured.

Heterodyne Force Microscopy

The sample is excited with ultrasound pulses from below. An ultrasound oscillation with a slightly different frequency is applied to the cantilever. When the ultrasound travels through the sample and reaches the tip, it will mix with the ultrasound in the AFM tip and will result in a signal at the difference frequency. Since parts of the sample with a different acoustic impedance, for instance impurities will scatter the ultrasound, the amplitude of this mixing signal in each position can be convoluted to find the locations of these impurities buried below the surface.

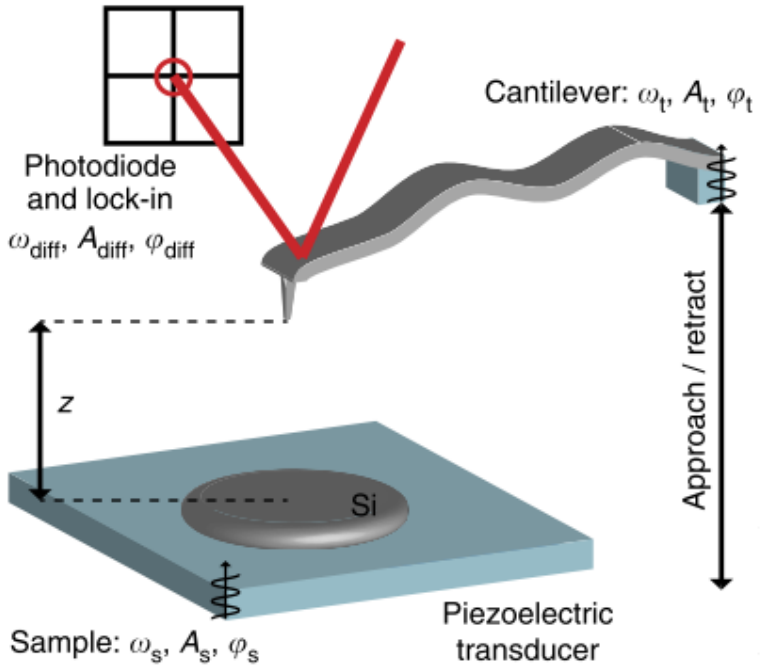

Figure 1.3: *Schematic of heterodyne force microscopy The cantilever tip is excited at frequency ω_t, amplitude A_t and phase ϕ_t, The sample is driven with ω_S, A_S and ϕ_s. The difference in z between the tip and the sample will vary with the difference of those oscillations. This distance scales with the interaction strength between tip and sample and the deflection of the cantilever. By measuring in multiple positions, the difference between this heterodyne signal holds information on how the ultrasound travelled through the sample, from which the subsurface structure can be deduced. Image is taken from [12].*

Ultrasound Force Microscopy

This is what we intend to achieve. It has not been experimentally shown yet. It has a lot in common with Heterodyne Force Microscopy. The main difference is we now measure a reflected ultrasound instead of the transmitted signal through the sample. This makes it possible to measure a broader set of samples. The subsurface structure up to a certain depth can be measured of thick samples that would fully attenuate the transmitted signal. Also, because a laser is used to actuate the cantilever higher frequencies can be used. GHz pulses will be applied to the backside of the cantilever to excite the ultrasound pulse. These high frequencies are used so Rayleigh scattering becomes the main cause in the contrast. These GHz pulses will propagate as ultrasound through the tip. From the tip, the ultrasound will go into the sample and propagate further. Again it will (partly) reflect upon parts with different acoustic impedances. The reflected signal will propagate back through the tip and will be read out optically. The time delay between the pulse and the arrival of the reflected signal back at the backside of the cantilever, where it will be de-

tected, is proportional to the distance from the impurity to the tip. This is kind of like echolocation on the nanoscale.

1.3 Frequency Stability

Before we can attribute changes in the frequency of the cantilever to interactions with a sample, we need to characterize the stability of the cantilever in the absence of a sample. A common way to express the stability of a system is through a standard deviation. However, resonators might experience a drift in frequency, which causes the classical standard deviation not to converge for increasing measurement time. This will therefore make the classical standard deviation useless for analysing frequency stability.

The same problem arises in characterising the precision of time-keeping devices. If a clock is off by one second a day, after a year the clock is more than 6 minutes out of sync with a perfect clock. Expressing this with the classical standard deviation will not make any sense.

To overcome these issues, David Allan introduced the Allan deviation in his masters thesis in 1965. The Allan deviation does not use the variance of the frequency itself but uses the variance of the change in frequency in a certain time interval instead. This makes the Allan deviation a function of this time interval.

Since the Allan deviation uses the difference between two points in time, the Allan deviation does converge for random walk like processes because the step size does not converge with time.

The Allan deviation, which is often plotted against the time interval, is an international standard for frequency stability. It is for instance used in atomic clocks and frequency stabilized lasers. It is also used to measure the bias stability of gyroscopes. In this report, it will be used for characterising the bias stability of the AFM cantilever. In the theory section, the Allan deviation will be described in more detail.

1.4 Thesis Outline

In this report we will discuss the general working principles of an AFM. Furthermore the theory of frequency stability using the Allan deviation will be developed for later use. Later we will describe how the different parts of this AFM are build up, and how we can use them to measure the frequency stability of a cantilever. In the results section, we will present the first measurements done with this AFM, which we will use for the peak detection to track the resonance frequency of the cantilever. We will also present and discuss the cantilever stability measurements. Finally, we will mention the current limitations of this setup and how we can overcome some of them.

CHAPTER 2
Theory

2.1 AFM

In AFM, to measure the forces a small beam is used. This cantilever deflects under a force, following Hooke's law.

$$F = kx \tag{2.1}$$

By measuring the deflection of the cantilever the force at the tip can be calculated. Since at the atomic scale, forces greatly scale with distance, the measured forces can be used to estimate the distance from the tip to the sample can be determined.

2.1.1 Modes of operation

The intermolecular forces between the cantilever tip and the sample vary greatly with distance. At short ranges, Pauli repulsion due to overlapping electron orbitals will cause a strong repulsion between the tip and sample. At longer ranges, van der Waals attraction between the sample and tip will occur. Other forces might also play a role at the larger distances, for instance electromagnetic forces.

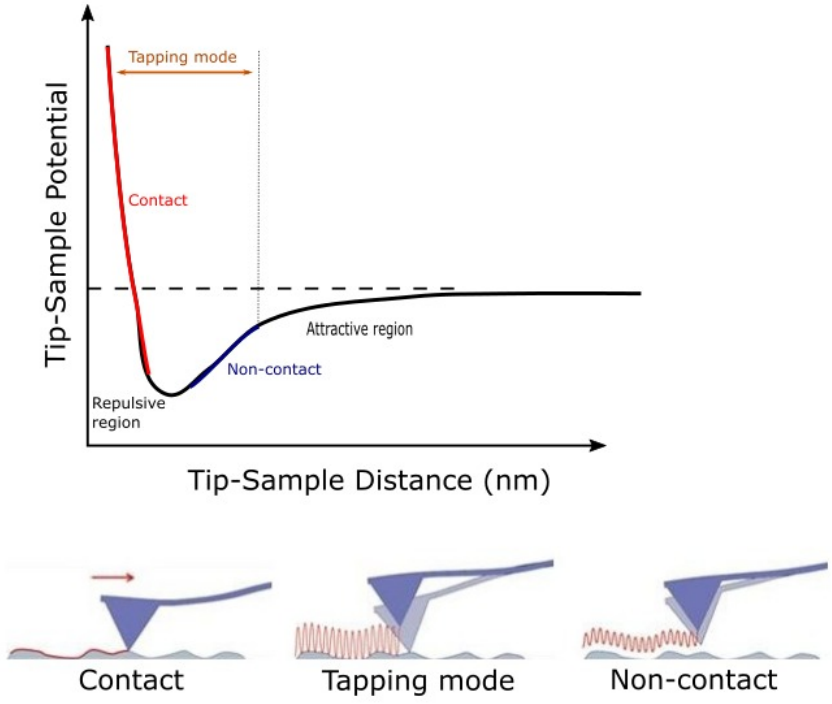

Figure 2.1: *Tip-sample potential. The force on the tip is equal to the slope of this potential. A negative slope pushes the tip away (repulsive region). A positive slope pulls the tip to the sample. In constant force of contact mode, the tip is continuously in contact with the sample and in the repulsive part of the potential. In tapping mode, the tip is tapping the surface every oscillation. The tip is moving forth and back between the attractive and repulsive region. In non-contact mode the tip is floating above the sample oscillating. Never leaving the attractive region.*

Constant Force Mode

In the most basic operation mode in AFM, constant force mode, the tip is kept in contact with the sample. Since the slope in the potential is steep (figure 2.1), small height differences cause a large force that bends the cantilever. A feedback system will change the separation between the cantilever tip and the sample to go back to the original height. Now the force is back at its starting point and the deflection will be at its bias again. By mapping the changes in height made to keep the deflection constant, the height of the sample can be mapped. This is a relatively fast way of measuring the height profile. However, since the slope is that steep, the forces can be enormous. This makes this method unsuited for soft samples since the cantilever tip will scratch and damage the sample.

Tapping Mode

To prevent this, the cantilever can be retracted a little and be driven at its resonance frequency above the sample. Now the cantilever will only touch the sample in some parts of the oscillation instead of continuously. Therefore this mode is called tapping mode. The forces can be kept much lower in this mode since we are in a less steep part of the potential. By using feedback to keep the oscillation amplitude or frequency constant, a heightmap of the sample can be made as well. While this method is more suited for softer samples, the measurements take much longer. This is because the cantilever has to oscillate a few times in each position to determine the amplitude or frequency for the feedback. Tapping mode AFM is also less suited for measurements in liquids since the liquid will dampen the cantilever oscillations.

Non-Contact Mode

It is also possible to measure by driving the resonance frequency of the cantilever without tapping the sample. This is called non-contact mode AFM. Since the forces will be even smaller than in tapping mode, the sample surface will remain undamaged and the AFM tip lasts much longer in this mode. However in general the resolution that can be achieved in this mode is much lower. Also, since due to the humidity a small meniscus of water will form on every sample, non-contact AFM measurements should be done in Ultra High Vacuum to prevent interference with this water layer.

E(R)FM and M(R)FM are examples of non-contact AFM that make use of the electric and magnetic interactions between the tip and the sample.

The measurements we are doing are without a sample, and can also be seen as non-contact measurements. However, no height feedback is used.

2.1.2 Photothermal Actuation

To drive the cantilever we will use another laser. The cantilever is made from silicon chip, with a metallic reflecting coating on top to reflect the laser beam, for measuring the deflection. These two materials have other thermal properties. If we use a laser of which part of the power gets absorbed by the cantilever, the cantilever will heat up and the different responses of the materials in the two layers will cause stress in the cantilever which will lead to bending. If we now modulate the laser power with the resonance frequency of the cantilever, the cantilever will periodically heat up and cool down, causing oscillations at the resonance frequency.

The heating of the cantilever will cause the cantilever to deform. The different thermal expansion coefficients (α) will cause both materials to expand in different ways. To now calculate how much force this expansion will apply to the rest of the cantilever we need the Youngs modulus. The Youngs modulus (E) is the stiffness of a material in the linear regime. It measures the force per unit area (stress) divided by the fractional deformation (strain) of the material. For a stiffer material (higher Youngs modulus), the resulting force applied to the non-expanding parts of the cantilever due to the thermal expansion will be higher.

This force will lead to a compression of the layers in the long axis of the

cantilever. Using the Poisson ratio of the material, the resulting expansion or compression in the perpendicular directions can be calculated.

Of course in the real world, one would get a gradient of temperatures within the cantilever, and a continuous bending as a result.

By doing a more exact analysis one could arrive at the following formula [7]:

$$F \propto \frac{h_1 h_2}{2h_1 h_2 + h_1^2 + h_2^2} \left(\frac{E_1 \alpha_1}{1 - \nu_1} + \frac{E_2 \alpha_2}{1 - \nu_2} \right) \tag{2.2}$$

Where h_i is the thickness of layer i, E_i is its Youngs modulus, α_i is the thermal expansion ratio and ν_i the elasticity of the layer.

To maximize the driving force for photothermal actuation, the two layers should have the same thickness. Furthermore, the materials should be chosen in such a way the thermal expansion ratio, Youngs modulus and Poisson ratio of the two materials should differ as much as possible.

The bending force on the cantilever also scales with the temperature and the surface of the heated spot. Since the temperature increase is determined by the amount of laser power absorbed by the cantilever and the specific heat of the material, we can drive the cantilever by modulating the laser power. This driving can be made more efficient by using a laser wavelength of which a large portion is absorbed by the cantilever.

Since the photothermal actuation is done at the cantilever itself, opposed to piezoelectric actuation which is done at the base of the holder, photothermal actuation should lead to a much cleaner spectrum, since only the resonance of the cantilever itself will be excited. For piezoelectric actuation, there is also the resonance frequency of the piezo itself, and the resonance frequency of the cantilever holder and other parts of the AFM, which results in a forest of peaks. Also, when using a laser to actuate the cantilever, the available frequencies are not bound by the resonance of the piezo. A much wider spectrum of frequency can be used. For us, this is particularly useful because in the future we want to actuate the cantilever at GHz frequencies, which is not possible using a piezo.

2.2 Frequency Stability: Allan Deviation

The Allan deviation [2] is a measure of frequency stability. This frequency stability is measured with respect to another oscillator. In this case, we will compare the frequency stability of an AFM cantilever to the internal oscillator of the lock-in. The Allan deviation is a dimensionless unit. The Allan deviation of a certain time interval can be interpreted as the fraction of the resonance frequency that is the RMS value of the frequency change after this time interval. Both short term stability and long time stability can be analysed. Long term instability is often caused by environmental factors, for instance temperature change.

2.2.1 Allan Variance

To be able to compare oscillators with different resonance frequencies in this analysis, we will introduce the fractional frequency error $y(t)$.

$$y(t) = \frac{\nu(t) - \nu_n}{\nu_n} \tag{2.3}$$

Here $\nu(t)$ is the actual frequency, and ν_n is the ideal frequency of the oscillator.

Now, before the Allan deviation can be calculated, we determine the average fractional frequency in an interval i. The average fractional frequency in the i^{th} interval of duration τ is the sum of all fractional frequencies within the interval divided by the length of that interval:

$$\bar{y}_i(\tau) = \frac{1}{\tau}\int_0^\tau y(i\tau + t)dt \tag{2.4}$$

To calculate the Allan Variance [13] the change in $\bar{y}$ from one moment in time to a time τ later is measured, This is squared and then averaged over some dataset. To make this variance equal to the classical variance for classical noise, this is further divided by 2.

$$\sigma_y^2(\tau) = \frac{1}{2}\langle(\Delta\bar{y})^2\rangle \tag{2.5}$$

The Allan deviation is the square root of the Allan variance. Since the Allan deviation and variance are functions of τ, They can be used to determine both the amplitude and the kind of noise. One of the most important features of the Allan deviation is that it can distinguish different noise types. Different kinds of noise will have a different scaling of Allan deviation with interval time τ.

Allan Variance response to different kinds of noise		
Noise type	Frequency noise	Allan deviation
White phase modulation	f^2	τ^{-1}
Flicker phase modulation	f^1	τ^{-1}
White frequency modulation	f^0	$\tau^{-\frac{1}{2}}$
Flicker frequency modulation	f^{-1}	τ^0
Random-walk frequency modulation	f^{-2}	$\tau^{\frac{1}{2}}$
Drift	f^{-3}	τ^1

Table 2.1: *The Allan deviation can distinguish different kinds of noise by the slope with τ on a log-log plot. However White phase modulation and Flicker phase modulation can not be separated using the Allan deviation. [13]*

The smallest time interval that can be used in a measured data set is the inverse of the sampling rate. Furthermore, only integer multiples n of this sampling time τ_0 can be used. For each time interval between the sampling time and the total measurement time $\frac{N}{\tau}$, with N the number of samples, we can write out the (non-overlapping) sum for the Allan variance:

$$\sigma_y^2(n\tau_0) = \frac{1}{2n(N-2)} \sum_{i=0}^{\frac{N-2}{n}-1} \left(\bar{y}_{(n+1)i}(n\tau_0) - \bar{y}_{ni}(n\tau_0)\right)^2 \tag{2.6}$$

We split the data set in equal blocks with n samples. For each block of n fractional frequencies, we calculate the average. Now we take the squared difference of the averages of two consecutive blocks and sum all of those. There are $N-2$ elements in this sum because of the fact that from N data points, we can compute $N-1$ averages with an interval length of $n\tau_0$. We can then take $N-2$ differences between those averages.

This is the square of the sum of two consecutive readings of the average fractional frequency error in a time interval τ, averaged over the data set. However, for each time interval $n\tau_0$ there will only be $\frac{N-2}{n} - 1$ of those intervals. The larger the time interval is, the lower the amount of data that is used to characterise the frequency stability at that time interval.

Overlapping Allan Variance

This problem can be solved by shifting all fractional frequency errors one index and calculating the average fractional frequency errors again. By doing this multiple times we will use multiple overlapping blocks of fractional frequency errors to calculate the averages. This leads to n generated subsets to calculate the Allan variance from. This is the Overlapping Allan variance.

$$\sigma_y^2(n\tau_0) = \frac{1}{2n^2(N-2n)} \sum_{j=0}^{N-1-2n} \left(\sum_{i=j}^{j+n-1} \left(\bar{y}_{n+i}(n\tau_0) - \bar{y}_i(n\tau_0)\right)^2 \right) \tag{2.7}$$

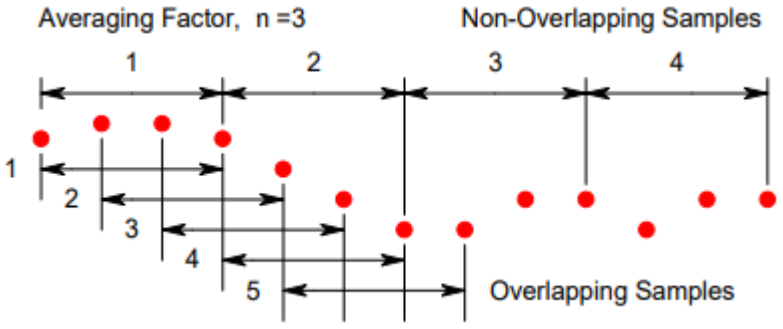

Figure 2.2: *The difference between the Allan deviation and overlapping Allan deviation. In the non-overlapping case, in this example for n=3, two possible averages (arrows) are skipped, since the new average is calculated from the next non-overlapping block of data. In the overlapping case, averages are calculated of overlapping blocks of data, leading to much more averages to use in the Allan deviation when n is becoming large [8].*

Since now more data series are used to calculate the Allan variance (figure 2.2), for larger interval times the performance of the overlapping Allan vari-

ance is superior to the non-overlapping one. However, it is slower to compute for large data sets.

Modified Allan Variance

To overcome the shortcoming the Allan variance can not separate white phase modulation and flicker phase modulation the modified Allan deviation was introduced. Both noises respond differently to bandwidth. By artificially reducing the bandwidth of the data, a new variance can be calculated that does separate them. This is the modified Allan variance [3].

CHAPTER 3
Methods

3.1 Setup

For the measurements presented in this thesis, we have used an old AFM that was home built in Leiden before 2007 [5]. The AFM is placed in an acoustic box to prevent acoustic excitation of the cantilever.

The AFM had not been used in the last decade and was disassembled and separated over different boxes. So we started to test the components to rebuild the AFM.

3.1.1 Optical Detection System

For the optical detection of the deflection of the cantilever, a 785nm laser is used. A red laser is used since shorter wavelengths might damage the sample. This laser is directed at the cantilever and reflected to an array of 16 photodiodes in a row. Deflection of the cantilever changes the spot where the laser hits the detector.

Aligning the optics

To get the maximum laser power to the detector via the cantilever we have to align the optics inside the AFM. This is done using five screws:

1. To move the fiber input up and down with respect to the optics.
2. To move the photodetector array forth and back with respect to the optics.
3. To move the focussing lens up and down
4. To move the optics forth/back with respect to the cantilever
5. To move the optics left/right with respect to the cantilever. This one is not visible in the picture since it is at the opposite side of the AFM.

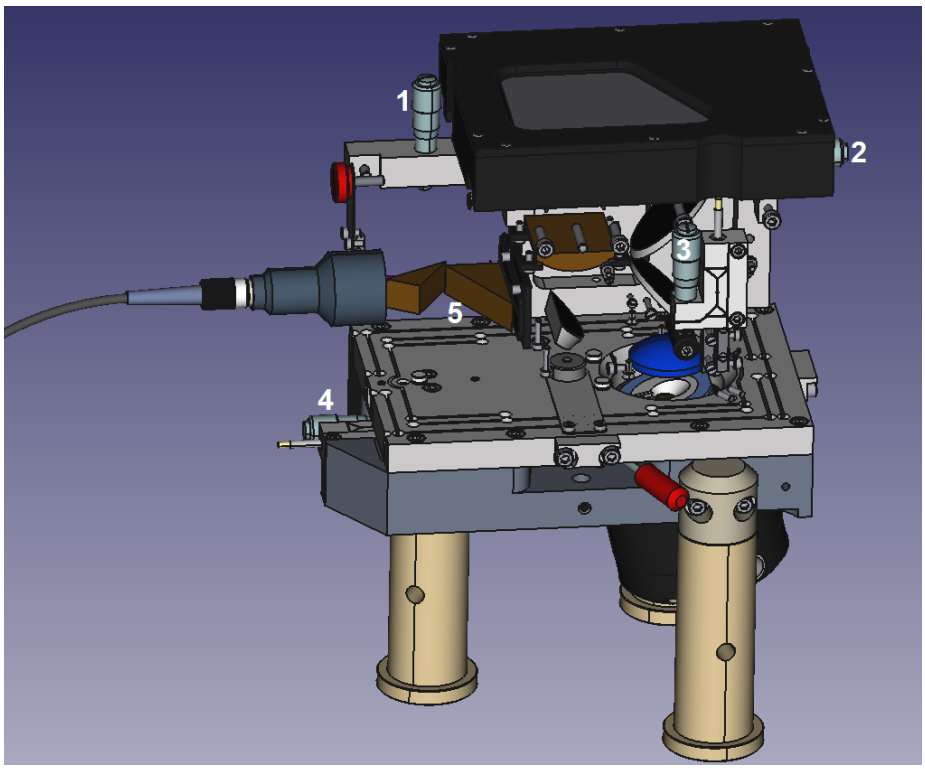

Figure 3.1: *Design of the AFM. Screws for aligning the optics are numbered. 1 moves the fiber input up and down. 2 moves the black part with the photodetector inside from left to right. 3 moves the dark blue focussing lens up and down. 4 moves the AFM with respect to the cantilever and 5 moves the AFM with respect to the cantilever in the perpendicular direction.*

Screw 1 and 2 are used to aim the laser beam at the cantilever. Screw 3 is used to focus the light on the cantilever so the maximum amount of laser power is reflected towards the detection chip. When 1 and 2 are used to change the relative position of the cantilever, one should refocus the light using screw 3 to maximise the signal.

Screw 4 can be used to align the center photodiode with the laser beam when the cantilever is out of contact to set up the deflection signal. It is also used to aim the beam at every photodiode one by one while tuning the gains of the weighted sum to correct for differences in sensitivity between the 16 photodiodes, which will be explained in the next section.

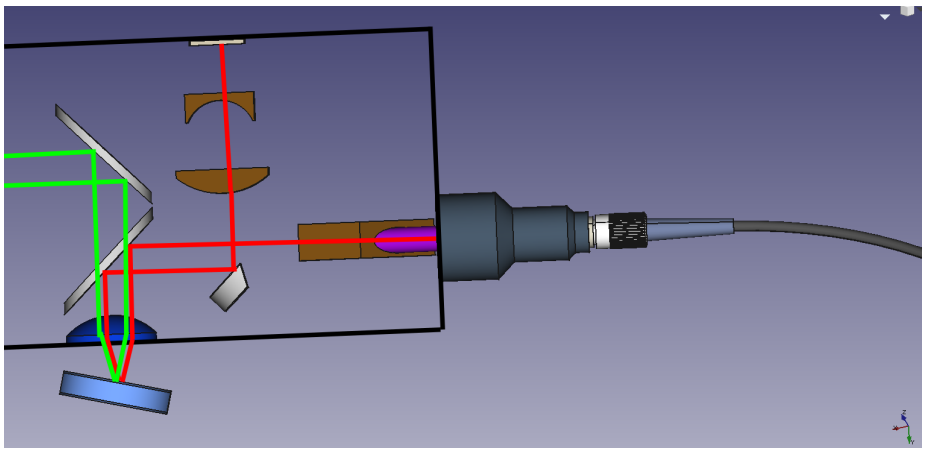

Figure 3.2: *Schematic of the optics inside the AFM. The lenses and mirrors are designed for a 785nm red laser.*

Figure 3.2 shows the paths of the laser beam when the optics are well aligned.

Reading out Photodiode signal

The photodiodes convert the optical power into a voltage. Within the AFM head, this voltage is amplified for the first time. Each photodiode has his own amplifier consisting of an opamp (Texas Instruments OPA657) with a $69k\Omega$ resistor. These amplifiers have a 10 MHz -3dB bandwidth. The maximum input per photodiode is $90\mu W$ and the maximum amplifier output is 3.5V [1].

The signal of each photodiode is read out with the analog inputs of two USB-DAQs (NI USB-6008) that are connected to the computer via USB. On this PC we can now visualise the readings of each of the 16 photodiodes to help with the alignment.

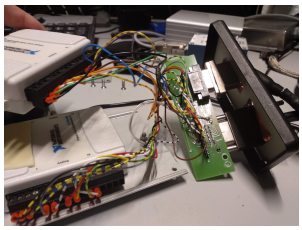

(a) *Opened box with USB-DAQs (NI USB-6008).*

(b) *USBDAQ box (almost) closed.*

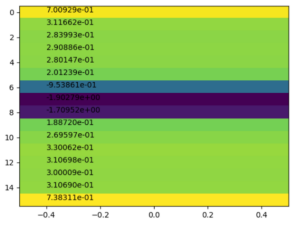

(c) *Example read of 16 photodiode signal on computer.*

Figure 3.3: *The USB DAQ box has 4 connections. (a) Two cables share the same connections to the analog inputs of the DAQs. One brings the signals from the photodiodes that are measured. The other one sends this signal in parallel to the summing module. (b) Both DAQs are connected to the computer via USB. (c) The signal from the 16 photodiodes is read out on the computer.*

Connecting the Photodiodes signal to the summing module

There is also a summing module. On this summing module. the polarity and gain of each photodiode signal can be set. This allows for adding or subtracting each signal with amplification up to 3 times to the weighted sum.

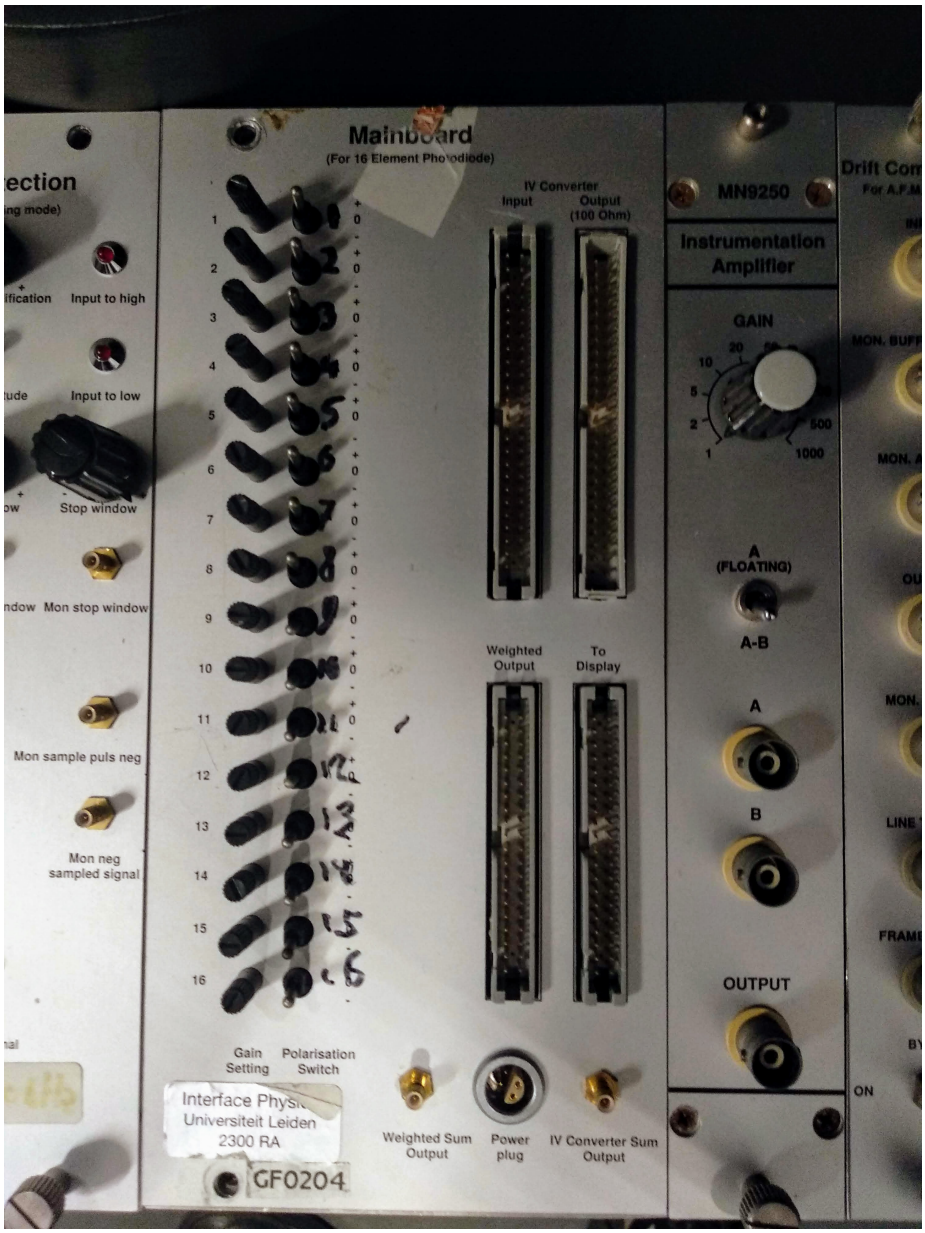

Figure 3.4: *Summing module. The signal from the 16 photodiodes goes into "Input". When the gain settings and polarisation switch are tuned accordingly, the weighted sum output is the deflection signal.*

This tunable gain is used to correct for sensitivity differences between the

different photodiodes. To get a signal that corresponds to the deflection of the cantilever the signal from the first 8 photodiodes needs to be added and the signal from the last 8 photodiodes has to be subtracted. This will give a positive signal when the laser spot hits the detector above the center and a negative signal when the laser spot hits the detector below its center.

However, there was no cable to make the connection between the summing module and the AFM head with the photodiodes. Also, the documentation was lacking a description of the pinout of the connectors.

Summing module side To determine which pins of the summing module we should connect, we measure the resistance of each pin. Most of them have a resistance of less than 1Ω between them. These are the grounds.

16 of the pins have a constant resistance to the grounds. These are the input pins for the 16 photodiodes. The resistance of each these input pins is $400 - 800\Omega$. However, when the polarity of one of the amplifiers is set to zero, its resistance changes to $1.2K\Omega$. This is used to measure which input pin connects to which amplifier.

Then there are two pins for which the resistance increases from 1 to 5 $k\Omega$ while measuring. This is the charging of a capacitor, that sits there to stabilise the output voltage. These pins are the power supply to the amplifier inside the AFM head. When the summing module is turned on, one of them supplies a +5V signal and the other one supplies a -5V signal.

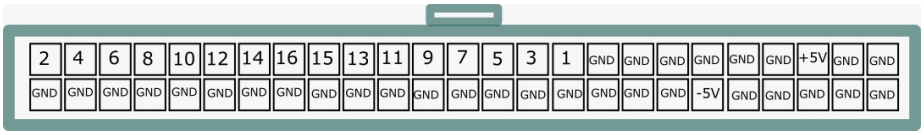

Figure 3.5: *Pin layout of input connector in summing module. The numbers refer to the corresponding amplifiers that can be tuned using the polarity switches and gain screws (figure 3.4).*

AFM head side The cable to connect the photodiodes inside the AFM head to the USB-DAQs was already supplied. We could measure which inputs from the USB-DAQ were connected to which pin in the connector. This made it possible to identify the order of two groups of 8 photodiodes since each USB-DAQ has 8 analog inputs. By visualising the voltages of the photodiodes on the computer and changing the laser spot position, we could determine which USB-DAQ reads the signal from the first 8 photodiodes and which one has the last 8. We found 4 of the pins were connected to the ground of the USB-DAQs.

That left 5 unknown pins remaining. The amplifiers inside the AFM head needs a power supply as well. Within these 5 pins, there were two groups of two interconnected pins. These had to be the +5V and -5V connections. Since the opamp (OPA657) used in the AFM head also accepts to reverse the polarities of the power supply, we have connected one group of 2 pins to the +5V and the other group to the -5V.

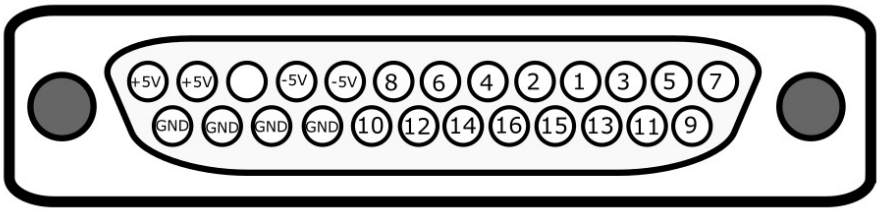

Figure 3.6: *Connector pin layout on the AFM head. The numbers refer to the photodiode position in the detector array, from top to bottom. The empty pin is unconnected.*

We have made a cable to connect each pin from this connector to the corresponding pin at the connector of the summing module.

Deflection signal: weighted sum of photodiodes

To get the deflection signal the gains have to be set appropriately to correct for sensitivity differences between the photodiodes.

The first problem that arose is that one of the amplifiers in the amplifier array in the summing box is broken. It gave a constant output of +5.8V independent of the laser intensity. This is the 11th amplifier in the array, which connects to one of the photodiodes close to the center, where during measurements most of the time the laser spot should be located. Therefore this was rewired so the 11th photodiode is amplified by the 16th amplifier in the amplifier array. Now the 16th photodiode remains unconnected. The polarity of the 16th amplifier is set according to the 11th photodiode and the polarity of the 11th amplifier is set to 0. Effectively the measurement is now done using only 15 photodiodes, but the gab is removed from the center to the edge of the photodiode array. To set the gains correct, the polarities of each of the signals are set to 0. This way the signals do not end up in the weighted sum. Now, we go over the photodiode signals one by one, setting their polarity correctly and remaining all other polarities zero. Now we use screw 4 (section 3.1.1) to move the detector so the laser gets aligned on this photodiode to get the maximum signal. The gain is now tuned to make the weighted sum a certain value. For instance +2V for all photodiodes where the polarity is positive and -2V when the polarity is negative. Since the USB-DAQs won't be affected by this change, The value read by the USB-DAQ for this photodiode is used to digitally normalise this signal later. When this is done all polarities can be set to their correct values, leaving the gains untouched. Now the optical detection system is ready for use.

3.1.2 Photothermal Actuation Laser

To drive the cantilever we plan to use a blue laser which we drive with the resonance frequency of the cantilever. In literature [7] for photothermal actuation of a cantilever, a 405nm 30mW laser was used. Based on this we ordered a 405nm 40mV laser (DL5146-101S). A Thorlabs LDC201CU driver and a TCC001 TEC controller will be used to control the laser current and temperature.

To mount this diode an old OFR T-E cooled Laser-to-Fiber Coupling System will be used. Since the laser diode sends out a divergent beam, a first collimator

is used to make a parallel beam. This parallel beam travels over an optical bench, on which there is space for an optical insulator to prevent reflections. We will not use this right away. By running the laser in constant current mode feedback should not be an issue that causes oscillations in the laser power. On the other end of the optical bench, the parallel beam will be focussed in a fiber that goes to the AFM. At the setup, the light from this fiber is again converted in a free space beam using another collimator. A beamsplitter is used to reflect the beam towards the mirrors in the AFM while still be able to visualise the cantilever using a digital microscope.

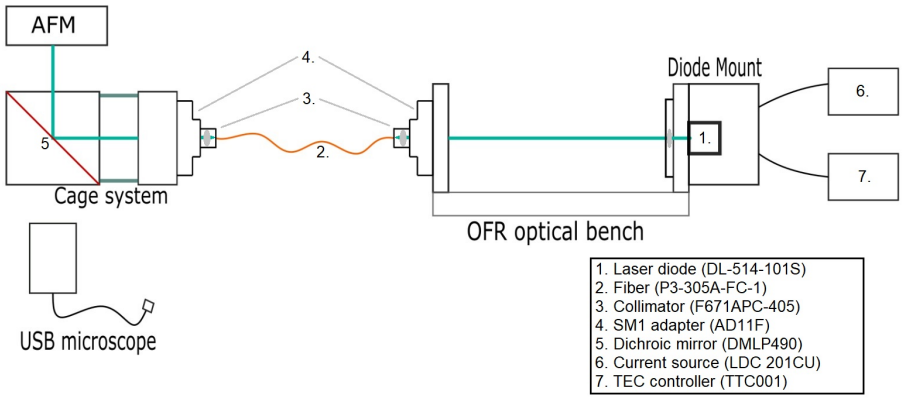

Figure 3.7: *Design of the 405nm laser with type indications for ordered parts.*

The parts have been ordered, but they did not arrive before the end of this project. We will continue with the photothermal actuation afterwards.

3.2 Piezo actuation

In the measurements presented in this thesis, a piezo will be used to drive the cantilever. Inside the cantilever is a small piezoelectric material. By applying a voltage, due to the piezoelectric effect, this material will expand. By making the piezo expand and shrink with the resonance frequency of the cantilever, the cantilever is driven. The cantilever holder rests with the two contacts of the piezo on contacts inside the AFM. However, these contacts were bent which made a connection impossible. Only after bending the contacts back and re-soldering the wire, we were able to use it to drive the piezo.

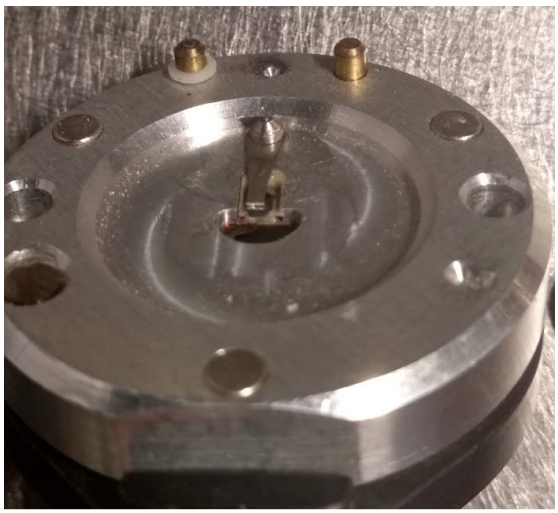

Figure 3.8: *Photo of the cantilever holder. Under the spring, the cantilever is glued in the holder using Crystalbond. Below this holder a small piezo is visible. The insulated gold pin at the top is the signal contact of the piezo. The other contact (right) is the piezo and holder ground. The 3 magnets are used to attach the cantilever holder to the AFM.*

3.3 Measurement procedure

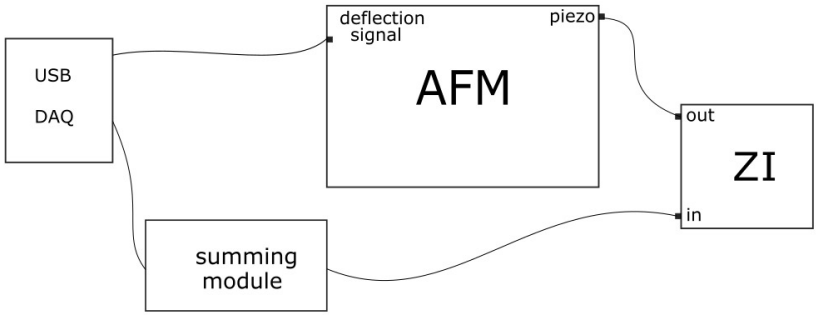

Figure 3.9: *The connections between the different modules in the setup: The deflection signal is routed to the box with USB-DAQs via a cable. There the signal is split in parallel between the USB DAQs, that read the voltage of each photodiode into the computer, and the cable to the summing module that takes the weighted sum. The weighted output from the summing module is connected to the input of the lock-in amplifier. The output from the lock-in goes to the piezo in the AFM to resonantly drive the cantilever.*

The red laser is aligned at the cantilever and driven with constant power (50mA). The response of the cantilever is measured using the detection system and the deflection signal is calculated using a weighted sum.

This deflection signal is attached to the input of a lock-in (ZI UHF). The output of this lock-in is connected to the piezo on the cantilever holder. A frequency sweep is done using this piezo. The resonance frequency of the cantilever is read from the response. The resonance frequency, Q factor of the peak and resonant phase are now used to set up a phase-locked loop (PLL) to track the resonance frequency in time. A PLL changes the output of the lock-in to keep the phase lag between input and output signal constant. The resonant phase is set in the PLL, after which the PLL will start to follow the resonance. This resonance frequency and the phase are recorded for a certain amount of time and the data is saved.

A python code is then used to calculate the Allan deviation from this dataset. This code generates a plot of Allan deviation vs time.

CHAPTER 4
Results and Discussion

In this chapter, the results of the measurements done in this project will be presented and discussed.

4.1 Thermal Peak

We first measured the spectrum without driving the cantilever. At 11kHz, a thermal peak was found. This peak became more clear when applying a higher laser power to the red detection laser, because of an increased signal to noise ratio.

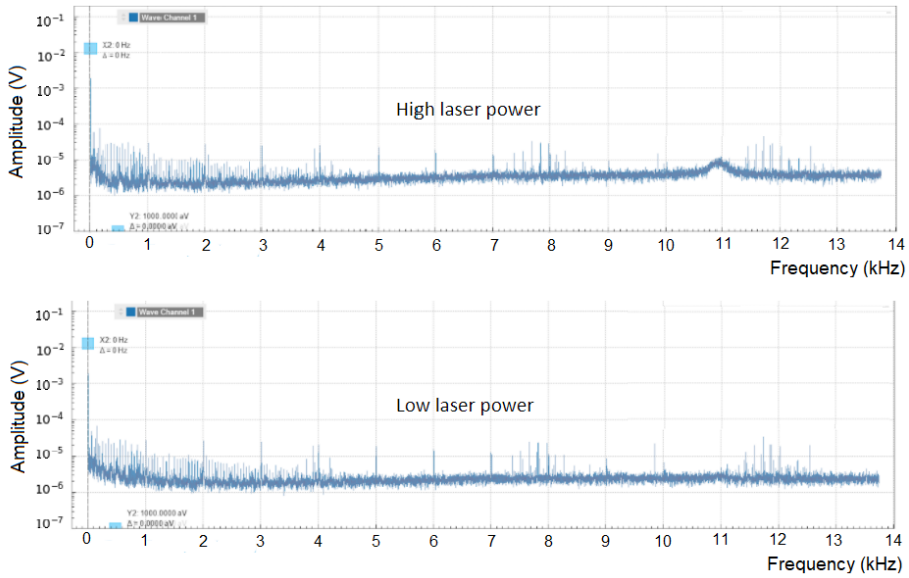

Figure 4.1: *Deflection signal without driving the cantilever. When the laser spot on the detector is strong enough to overcome the noise, the thermal peak is visible at around 11kHz. It has an approximate width of 500Hz, which gives a Q-factor of around 22.*

Using the equipartition theorem, since all degrees of freedom store $\frac{1}{2}k_bT$ of

energy, the theoretical amplitude of the thermal motion of the cantilever can be calculated using

$$\frac{1}{2}k_bT = \frac{1}{2}kx^2 \tag{4.1}$$

for a cantilever stiffness k of 0.04N/m, a temperature of 293K and using that the Boltzmann constant $k_b = 1.38064852 * 10^-23J/K$ this gives an amplitude for the thermal motion of 0.3nm.

This could be used as a benchmark. In figure 4.1, the read-out laser was driven at 50mA. With a resulting peak height of $8 * 10^{-6}V$, this yields a sensitivity of $37.5nm/mV$ when the read-out laser is driven at 50mA. However, the stiffness of the cantilever is not precisely specified. The box states 0.02-0.77 N/m. Therefore this analysis can't be used for this cantilever.

4.2 Frequency stability of Cantilever

To find the exact resonance frequency of the cantilever we performed a sweep. From the thermal peak, we already knew the peak should be around 11kHz. A peak to peak amplitude of 1.2V was used for the output. Make sure the input impedance of the lock-in is not at 50Ω and is DC-coupled. Otherwise, the kHz frequency of the cantilever will completely be filtered out of the signal.

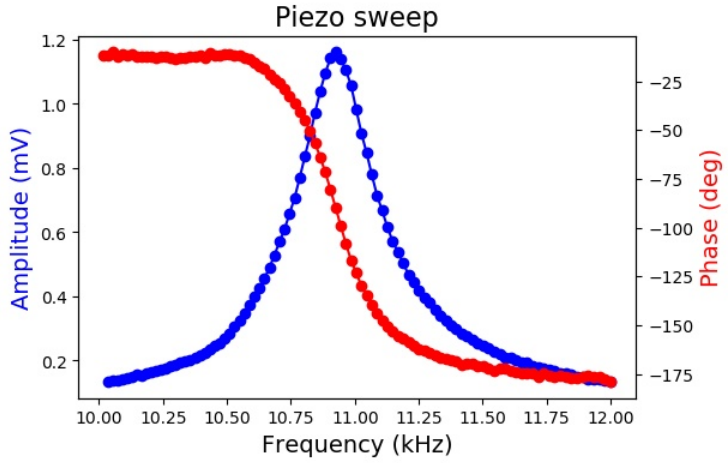

Figure 4.2: *Deflection signal response from frequency sweep between 10 and 12KHz on piezo at 1.2V peak to peak amplitude. An attenuator was used in the ZI input. The resonance frequency is 10.93kHz. The Q factor is 45.4. The phase lag between the input and output at resonance is -91.5 degrees.*

From the sweep the resonance frequency, Q-factor and resonant phase were calculated. These values were used to set up the phase-locked loop.

In the PLL settings, we set the phase setpoint, the center frequency and the upper and lower limit for how far from the center frequency the PLL is allowed to go based on the performed sweep. We move these values to the advisor, set an appropriate bandwidth and let the advisor set the correct proportional,

integral and differential feedback to lock the PLL. This is a bit of trial and error and should sometimes be repeated multiple times until the PLL locks. The bandwidth setting tells the PLL how fast it should try to follow the resonance frequency. Then we can go to the plotter to see the resonance frequency against time. We need to add a frequency to the vertical axis group and then select Demod1 sample frequency.

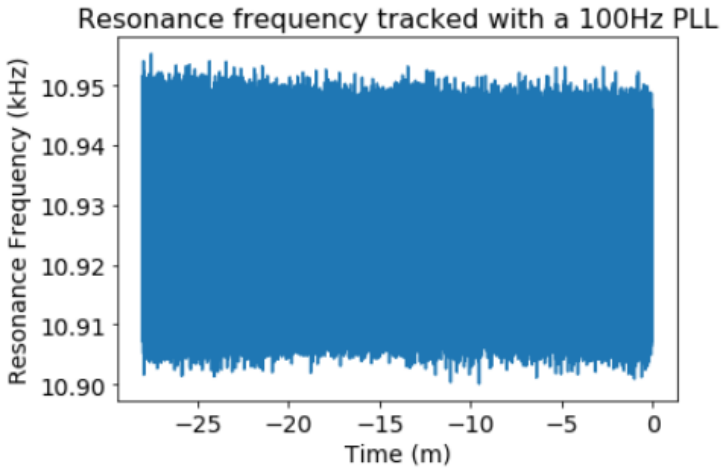

Figure 4.3: *PLL tracking the resonance frequency of the cantilever for 30 minutes. Lock-in output amplitude was 1.2V peak to peak.*

4.2.1 Allan Deviation

From this resonance frequency vs time data, the Allan deviation was calculated. For this, we used the Allantools python package. First, form the resonance frequency data we calculate the normalized resonance frequency y (equation 2.3). From the time data, we get the data rate. Using these the Allan deviation as a function of interval time τ was calculated. We have measured with a PLL bandwidth of 1000Hz for 5 minutes, a bandwidth of 100Hz for 30 minutes and 10Hz for 100 minutes. The resulting Allan deviations are plotted in the same figure.

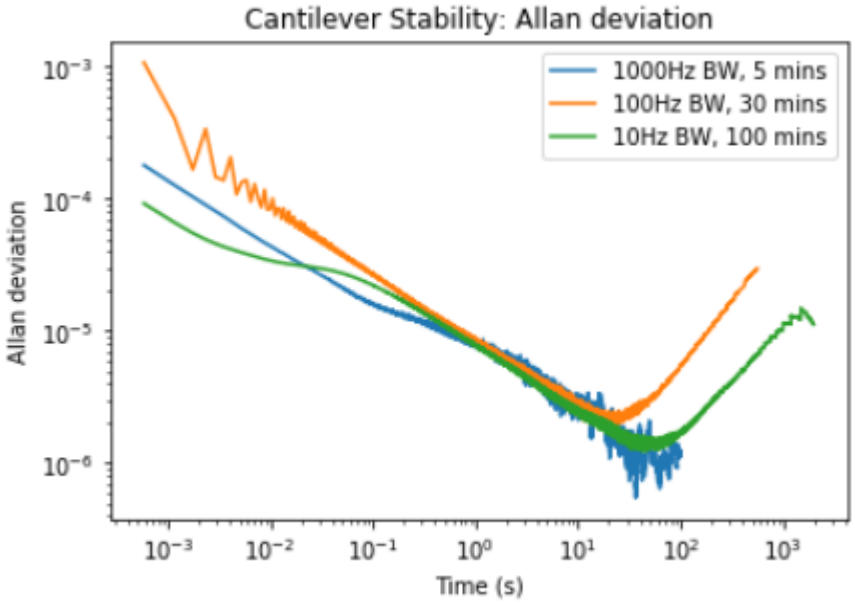

Figure 4.4: *Allan deviation plot for this cantilever. Interval times τ between $1/BW$ should not be interpreted. An Allan deviation of 10^{-6} at the dip at 100s means the RMS instability of two readings 100s apart is 10^{-6}. For a resonance frequency of 11kHz, this is 11mHz RMS. Two things stand out in this figure: For 1000Hz bandwidth, the Allan deviation is lower for shorter time intervals, and the upward slope for 100Hz BW starts at a shorter time interval than the other two.*

Because some of the cables in the optical detection system have not been shielded yet, sometimes random spikes are visible in the signal of a single photodiode. This also leads to random spikes in the deflection signal. We think these also cause spikes in the deflection signal. When measuring with a bandwidth of 10 or 100 Hz, these spikes are not visible in the resonance frequency. However when we measure with a bandwidth of 1000Hz these spikes become apparent.

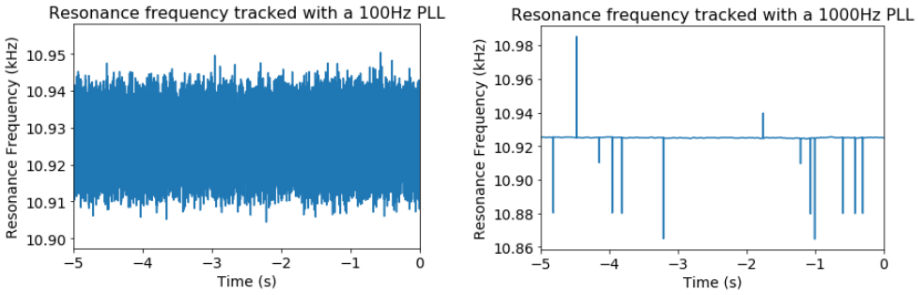

(a) *Resonance frequency tracked using 100Hz PLL*

(b) *1000Hz PLL used to track resonance frequency.*

Figure 4.5: *By using a 100Hz bandwidth for the PLL the spikes get lost in the data. Using a high enough PLL bandwidth (1000Hz) the spikes in the signal become clearly visible. Because the flatter data will mostly filter out the spikes in the Allan deviation, in figure 4.4 the 1000Hz BW has a lower Allan deviation than the 100Hz BW. Shielding all cables might remove the spikes and solve this issue.*

For the lower bandwidths, these spikes are part of the data and for 1000Hz bandwidth, these spikes are clear outliers and get averaged out more by the more apparent flat data. In figure 4.4 this results in the 1000Hz line having a lower Allan deviation for short time intervals.

For the interval times that get close to the total measurement time, there are fewer intervals to calculate the Allan deviation. By using the overlapping Allan deviation (section 2.2.1) the number of samples with this larger τ can be greatly increased. Leading to a lower noise in the Allan deviation plot.

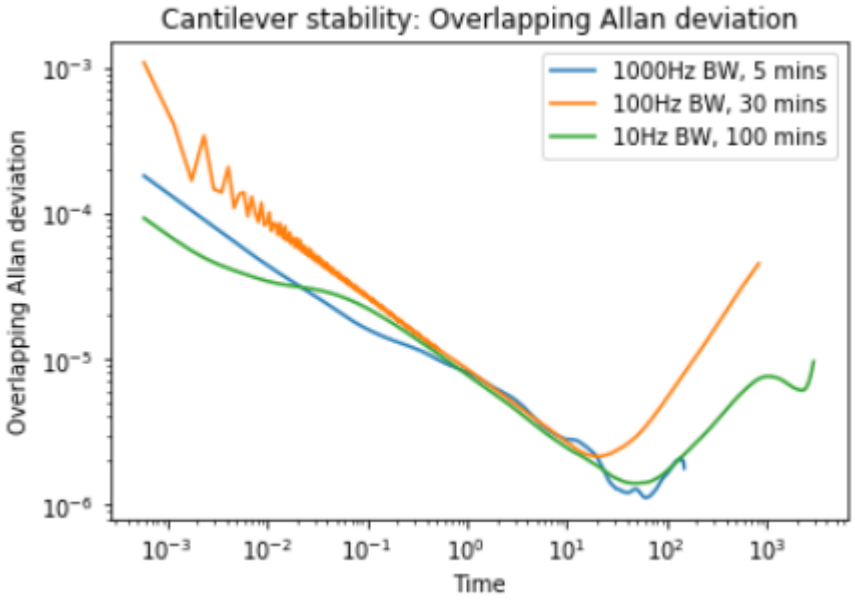

Figure 4.6: *The Overlapping Allan deviation plot for this cantilever. For longer time intervals the noise is greatly reduced compated to figure 4.4.*

The downwards slope in figure 4.6 of $-\frac{1}{2}$ means that the noise here is dominated by white frequency modulation. The upwards slope of +1 corresponds to a (non-random) drift in resonance frequency [6].

The minimum Allan deviation of 10^{-6} in figure 4.6 corresponds to a RMS frequency shift of 11 mHz for the 11kHz cantilever, or a 0.18mdeg phase noise ($\frac{11mHz}{11kHz} * 180$). In heterodyne force microscopy, a 50nm gold-particle buried at a depth of 200 nm in a soft polymer will already have a higher phase contrast at 1MHz. [11]

4.3 Literature Comparison

The cantilever we use has a length of $450\mu m$, a width of $50\mu m$ and a thickness of $2\mu m$. Since the density of silicon is $2.33g/cm^3$, the approximate mass of our resonator is $1.05 * 10^-7g$.

In [10], the resonator mass is compared to experimental data on their Allan Deviation, and the thermomechanical noise limit of these experiments.

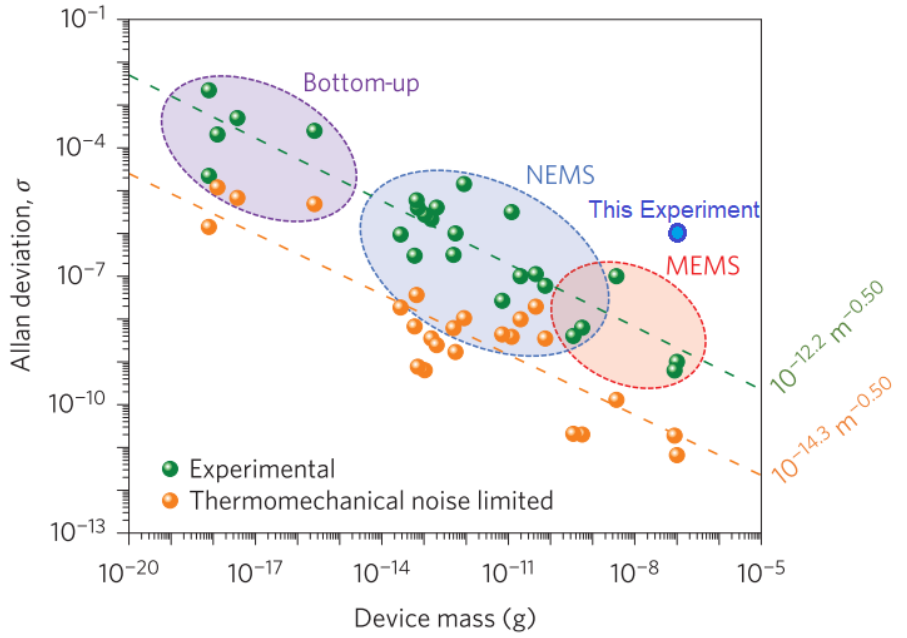

Figure 4.7: *Allan deviation vs resonator mass with our measurement added to the comparison figure from [10]. As expected our noise is higher than other experiments. Part of which can be explained by our unshielded cables.*

In figure 4.7 we compare our measurements to the literature. It is clear that our experiment can still be improved by a lot. Yet it is remarkable that even using unshielded cables, it is possible to track the frequency with a stability of up to 10^{-6} for a 100s period.

CHAPTER 5
Conclusion

We have tested the components of the old AFM and most of it is still using. However, one of the amplifiers inside the weighted summing module is broken.

We reverse-engeneerded the pinout of the connectors in the summing module and the AFM head and made a cable between them to get the optical detection system to work. Using this we were able to measure the thermal motion of the cantilever.

The connections to the piezo inside the cantilever holder are fixed and the cantilever can now be driven using a piezo.

Using both we measured the frequency stability of the cantilever. We found a minimum Allan deviation of 10^{-6}, which corresponds to an 11mHz RMS movement in resonance frequency. Comparing to the literature [10], we are 3 orders of magnitude less stable than a resonator with a comparable mass.
For interval times shorter than 30 seconds, where this minimum in Allan deviation is at, the changes in resonance frequency are dominated by white frequency modulation. For a PLL bandwidth of 1000Hz, this noise was lower than for a 100Hz PLL bandwidth. Zooming in at the signal showed spikes in the resonance frequency while measuring with a high enough bandwidth (1000Hz). These spikes are caused by the unshielded cable, so shielding all cables in the setup will improve the reading of the stability with a shorter interval time than 30 seconds and lower the part of the Allan deviation plots with the negative slope. For a time interval longer than 30 seconds, the slope in the Allan deviation is +1, which corresponds in a drift in resonance frequency.

CHAPTER 6
Outlook

The biggest improvement of the current working part of the setup would be to shield the cables. This was not our main priority during this project since the main goal was to get a signal at all. Now that we have a signal and can measure the frequency stability, this is the first thing that should be done.

Another improvement we want to make shortly is to add a blue laser (section 3.1.2) to the setup to be able to thermomechanically actuate the cantilever. This actuation is done at the cantilever itself opposed to at the base of the cantilever chip, as is currently the case with the piezo.

The 11th amplifier of the summing box is broken and should be fixed. It might be possible to fix it by just replacing the opamp with a new one. Then we will again have all 16 photodiodes to measure the deflection signal instead of the 15 currently in use. The summing module is part of a large rack, of which nothing else is in use. To gain more space around the setup, we should make this summing module a separate box independent of this rack.

I only measured the Allan deviation with an output amplitude of 1.2V. It would be interesting to repeat the measurement using a higher output amplitude to see if the frequency stability changes.

Bibliography

[1] D. W. Allan, N. Ashby, and C. C. Hodge. "The science of timekeeping." In: *Hewlett Packard application note 1289* (1997), pp. 1–88. URL: http://www.allanstime.com/Publications/DWA/Science%7B%5C_%7DTimekeeping/TheScienceOfTimekeeping.pdf%7B%5C%%7D5Cnhttp://literature.agilent.com/litweb/pdf/5965-7984E.pdf.

[2] David W. Allan. "Statistics of Atomic Frequency Standards." In: *Proceedings of the IEEE* 79.7 (1966), pp. 936–942. ISSN: 15582256. DOI: 10.1109/5.84970.

[3] David W. Allan and James A. Barnes. "A Modified "Allan Variance" with Increased Oscillator Characterization Ability." In: 53 (1983). ISSN: 1098-6596. DOI: 10.1017/CBO9781107415324.004.

[4] G. Binning, C. F. Quate, and CH. Gerber. "Atomic Force Microscope." In: *Physical Review Letters* 56.9 (1986), pp. 930–934. DOI: 10.1201/9781420075250.

[5] Allard Katan. *Measuring interactions in fluids with small-cantilever AFM*. 2007. ISBN: 9789090225746.

[6] Claudia C Meruane Naranjo. "Analysis and Modeling of MEMS based Inertial Sensors." In: *Work* (2008).

[7] Maarten E. van Reijzen et al. "Improved sub-surface AFM using photothermal actuation." In: July 2019 (2019), p. 19. DOI: 10.1117/12.2515441.

[8] W J Riley. *Handbook of Frequency Stability Analysis*. Vol. 31. 1. 1994, A49. ISBN: 3019753058. DOI: 10.1016/0148-9062(94)92706-5.

[9] D. Rugar et al. "Single spin detection by magnetic resonance force microscopy." In: *Nature* 430.6997 (2004), pp. 329–332. ISSN: 00280836. DOI: 10.1038/nature02658.

[10] Marc Sansa et al. "Frequency fluctuations in silicon nanoresonators." In: *Nature Nanotechnology* 11.6 (2016), pp. 552–558. ISSN: 17483395. DOI: 10.1038/nnano.2016.19.

[11] *Unravelling heterodyne force microscopy*. Leiden University Press, 2013.

[12] G. J. Verbiest and M. J. Rost. "Beating beats mixing in heterodyne detection schemes." In: *Nature Communications* 6 (2015), pp. 1–5. ISSN: 20411723. DOI: 10.1038/ncomms7444. URL: http://dx.doi.org/10.1038/ncomms7444.

[13] Martin H. Weik. "Allan variance." In: *Computer Science and Communications Dictionary* (2000), pp. 37–37. DOI: 10.1007/1-4020-0613-6_492.